International Journal of Engineering Research and Technology. ISSN 0974-3154, Volume 13, Number 12 (2020), pp. 4799-4803

Instrumental Distortion Correction Method for the ETM + Scanner on Landsat-7 Multispectral Satellite Images

[1]Dmitriy Mozgovoy[a,E], [2]Roman Tsarev[b,C,F], [3]Dmitriy Svinarenko[a,G], [4]Aleksey Danichev[b,H], Andrey Karnaukhov[d,I]

[A]Oles Honchar Dnipro National University, Dnipro, Ukraine.

[B]Siberian Federal University, Krasnoyarsk, Russia.

[C]Krasnoyarsk State Agrarian University, Krasnoyarsk, Russia.

[D]Reshetnev Siberian State University Of Science And Technology, Krasnoyarsk, Russia.

Abstract

An alternative instrument distortions correction method for the ETM + scanner on Landsat-7 multispectral satellite images is proposed. The method is based on the filtering application in the field of spatial frequencies using the fast Fourier transform and spectral masks. The visual analysis results of the processed images showed a high-quality suppression of instrument distortion of the ETM + scanner compared to other methods. Experimental testing of the proposed method on many images confirmed the good repeatability and high stability of the algorithms used. The developed technology can also be successfully used to correct instrumental spatial periodic distortions in archived satellite images obtained using other optical and mechanical scanners.

Keywords: Landsat-7 satellite, ETM + scanner, multispectral images, instrumental distortions, fast Fourier transform, spectral masks

INTRODUCTION

In recent decades, satellite survey has become the most widespread and affordable spatial data source in various fields of human activity due to its many advantages compared to ground-based survey methods [1-3]:

- maximum objectivity and reliability (satellite images can eliminate the people's mistakes, as well as intentional distortion or silence of important information).
- wide visibility and high information content (it is possible to survey any, even inaccessible territory on Earth with a coverage of thousands of kilometers).
- maximum relevance and high efficiency (the ability to deliver data to the user without delay - direct reception to subscriber stations).
- high frequency of survey (up to several images per day).
- multidisciplinarity (using the same images for solving a wide range of scientific and applied problems in the interests of various government agencies and private companies).
- the multispectral survey (survey in several spectral channels in the visible and infrared ranges).
- absolute safety (lack of risks to human health and life compared to ground methods).
- high economic efficiency (significantly lower costs compared to ground methods).
- maximum availability (ease of data obtaining and the absence of legal or political barriers).
- high confidentiality (stealth survey and minimizing the risks of information leakage).

An additional significant advantage of remote sensing data is open and free access to multispectral and radar satellite images of medium spatial resolution Landsat-7, Landsat-8, Sentinel-1A / B, Sentinel-2A/B, etc. [4-6].

Archival satellite images obtained by optical-mechanical scanners are often used to evaluate anthropogenic and natural changes in the earth's cover [7–9]. A distinctive feature of such images are various instrumental geometric and radiometric distortions. One type of instrumental distortion is radiometric interference with a spatial periodic structure. These interferences can be caused by various factors, among which are the following:

- a significant variation in the sensitivity and non-linearity of the sensor photocells (Landsat-5, Ocean-O satellites).
- different values of the gain and dynamic range of the amplification path elements (Sich-1 satellite).
- failures in the systems of data processing, transmission and storage (Landsat-3, Landsat-5 satellites).
- malfunctions of the on-board scanner mechanical elements (Landsat-7 satellite).

Among the abovementioned satellites, only Landsat-7 launched in 1999, is currently operating in orbit. On May 31, 2003, the SLC (Scan Line Corrector) corrector, which is one of

the key elements of the ETM + (Enhanced Thematic Mapper Plus) imaging system, failed on this satellite. Owing to this breakdown, the characteristic oblique black lines appeared in the entire image area in all spectral channels except the thermal one, expanding toward the edge of the image (Fig. 1). Only the narrow part of the image in the center of the scene remained undistorted (Fig. 2).

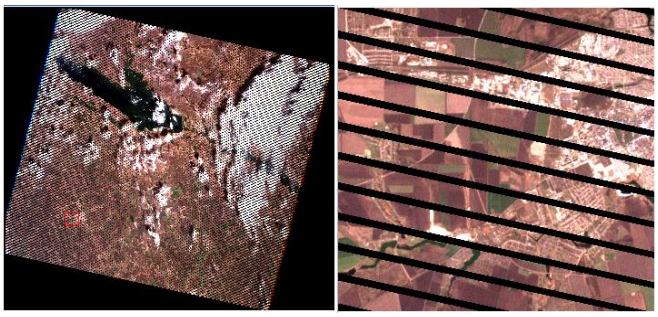

Fig. 1. Landsat-7 satellite image dated March 28, 2020
(left - full scene, right - enlarged fragment)

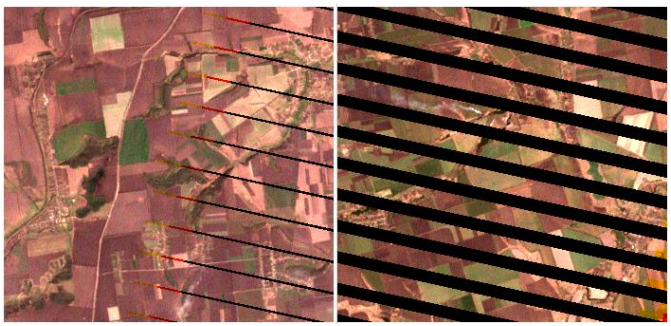

Fig. 2. Fragments of the satellite image Landsat-7 dated March 20, 2020
(left is the center of the scene; right is the edge of the scene)

The instability in time of the on-board scanner parameters (especially during abnormal operation) does not allow to automatically compensate for instrument distortions of this class directly on the satellite's board or at the preliminary processing stage of satellite images. The most effective instrument noise elimination algorithms work only with abnormalized images that preserve the original line structure (i.e., are not resampled with geometric correction and geographical reference). However, multispectral images of medium spatial resolution from Landsat-7, Landsat-8 and Sentinel-2A/B satellites are delivered to users only in normalized form.

Modern software packages for processing satellite images have a wide range of tools to eliminate different distortion types. However, using standard convolutional and morphological filters to eliminate interference with a spatial periodic structure in resampled images, is ineffective. Rank, majority, and median filters do not provide sufficient noise suppression. Smoothing and low-pass filters reduce the spatial resolution of the image, and directional filters introduce significant non-linear radiometric distortion.

To correct instrument distortions in the images from the Landsat-7 satellite, many methods and algorithms were developed [10-17], which then were programmatically implemented in various programming languages (C ++, Python, IDL, etc.). These algorithms were included in popular satellite imagery processing programs (ERDAS, ENVI, etc.), as well as in GIS packages (ArcGIS, QGIS, etc.). However, all these algorithms had significant disadvantages, such as:

- the need to use ready-to-use instrument distortion masks.
- work only with the whole scene (long processing time).
- many manual settings for processing procedures.
- additional images use in the same territory for other nearest dates, which is not always possible due to the presence of cloudiness or snow cover on them (Fig. 3).

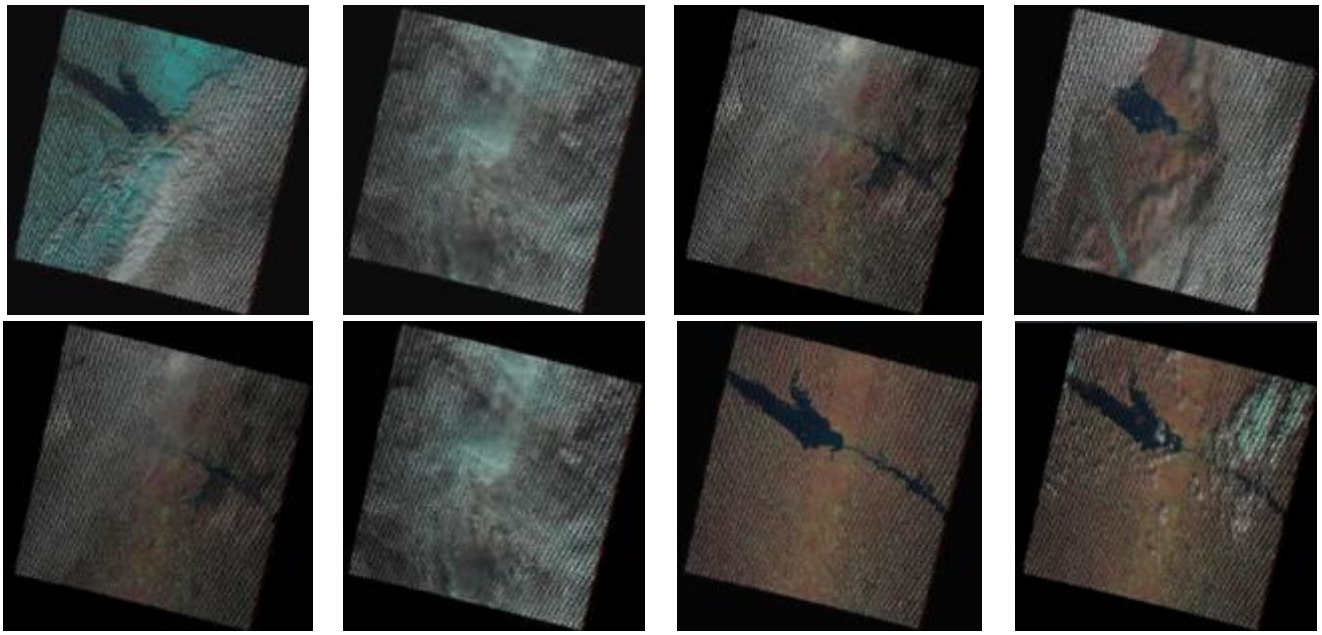

Fig. 3. Images from the Landsat-7 satellite dated December 2019 ... March 2020

(only one scene without cloud cover and snow cover)

The abovementioned disadvantages of existing methods do not allow or significantly limit their use in modern web services for online processing of satellite images.

The main objective of the research is the development and experimental testing of methods and algorithms for eliminating interference with a spatial periodic structure in satellite imagery.

Basic requirements for the developed methods and algorithms are as following:

- the ability to work without the use of masks instrument distortion.
- work with single-channel and multispectral images.
- the ability to work with small fragments of the scene.
- minimum number of manual settings for processing procedures.
- the ability to work without additional images for other dates.
- high stability of the algorithms using images from various satellites.
- good repeatability on satellite images taken in different seasons and for different territories.

METHODS

The spatial frequency of instrumental interference from optical and mechanical scanners allows to effectively filter them in the field of spatial frequencies using the mathematical apparatus of spectral analysis and synthesis, for example, the two-dimensional Fourier transform [18].

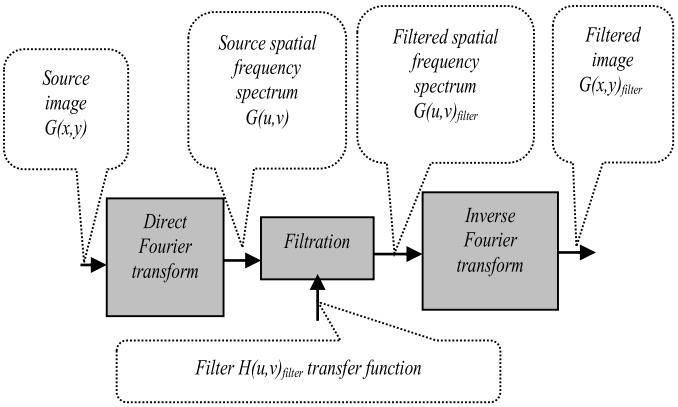

Fig. 4

When using the Fourier transform, filtering consists of the following operations (Fig. 4):

a) A transition is made from the spatial representation of G (x, y) to the spatial-frequency representation of G (u, v) by means of the direct Fourier transform:

$$G(\mathrm{u},\mathrm{v}) = \int_{-\infty}^{\infty}\int_{-\infty}^{\infty} \mathrm{G}(\mathrm{x},\mathrm{y})\exp[-2\pi\, i\,(\mathrm{u}\,\mathrm{x}+\mathrm{v}\,\mathrm{y})]\mathrm{dx}\,\mathrm{dy};$$

b) Filtering (removal of periodic interference) in the frequency domain is performed by multiplying the initial spectrum *G (u, v)* by the transfer function of the filter $H(u, v)_{filter}$ (mask with zero values in the spatial frequency range of the interference with u_{int}, v_{int} and unit values in the rest spatial frequency domain):

$$G(u,v)_{\,фильтр} = G(u,v)^{*}\, H(u,v)_{\,фильтр};$$

c) The inverse Fourier transform is performed to return from the spatial-frequency representation of the $G(u, v)_{filter}$ to the spatial $G(x, y)_{filter}$:

$$G(\mathrm{x},\mathrm{y})_{\text{фильтр}} = \int_{-\infty}^{\infty}\int_{-\infty}^{\infty} \mathrm{G}(\mathrm{u},\mathrm{v})_{\text{фильтр}} \exp[2\pi\, i\,(\mathrm{u}\,\mathrm{x}+\mathrm{v}\,\mathrm{y})]\mathrm{du}\,\mathrm{dv},$$

The parameters of the $H(u,v)_{filter}$ mask are determined by the known spatial period of the interference or experimentally by the filtering results. To represent digital raster images in the field of spatial frequencies (constructing a Fourier image of *F(u, v)*), a discrete two-dimensional direct Fourier transform is used:

$$F(\mathrm{u},\mathrm{v}) = \sum_{x=0}^{M-1}\sum_{\mathrm{y}=0}^{\mathrm{N}-1} [\,\mathrm{f}(\mathrm{x},\mathrm{y})\exp(-\mathrm{i}\,2\pi\mathrm{ux}/\mathrm{M} - \mathrm{i}\,2\pi\mathrm{vy}/\mathrm{N})],$$

where: *M* and *N* are the number of pixels of the original image horizontally and vertically, respectively, *i* is the imaginary unit, *u, v* are spatial frequency variables.

To speed up the calculations, the fast Fourier transform algorithm is used, which for N samples reduces the number of pairs of multiplication / division operations from $2N^2$ to $N\,log_2 N$. Before using it, the pixel size of the image is reduced to a square with a pixel size of 2^n x 2^n by highlighting part of the image or adding pixels with zero values.

To perform filtering on the spatial frequency area for removal, a filtering mask consisting of pixels with zero values is imposed (i.e., the corresponding elements of the Fourier image are assigned a zero value).

The spatial frequency variables *u, v* take both positive and negative values, which are located symmetrically on the Fourier image relative to the origin, which requires appropriate symmetry when applying a mask.

If necessary, low-frequency or high-frequency filtering can be performed in parallel with spatial-periodic interference filtering by adding appropriate masks.

To return to the raster image *f (x, y)*, the inverse two-dimensional Fourier transform is performed:

$$f(\mathrm{x},\mathrm{y}) = (MN)^{-1}\sum_{u=0}^{M-1}\sum_{\mathrm{v}=0}^{\mathrm{N}-1} [\,\mathrm{F}(\mathrm{u},\mathrm{v})\exp(\mathrm{i}2\pi\mathrm{ux}/\mathrm{M} + \mathrm{i}2\pi\mathrm{vy}/\mathrm{N})],$$

where: $x = \{1 \ldots N\}$; $y = \{1 \ldots M\}$– the pixel coordinates of the original digital image elements horizontally and vertically, respectively.

Periodic components whose spatial period corresponds to the spatial frequencies filtered on the Fourier transform will be removed in the filtered image. Filtering quality is determined by the mask applied.

RESULTS AND DISCUSSION

The results of image processing from the Landsat-7 satellite dated March 28, 2020 are shown below as an example (see Fig. 1). Since the image had cloudy areas, several fragments of 512x512 pixels in size were selected for testing from different places in the scene. One of the selected sections is shown in Fig. 5 (left).

The image *F(u, v)* obtained as a result of a two-dimensional direct Fourier transform, is normalized (amplitude scaling) for display in the mode of 256 gradations of gray [19]:

where: *F(u,v)* - pixel value after direct Fourier transform.

$F(u,v)_{max}$ – maximal pixel value.

$F(u,v)_{норм}$ – normalized (displayed) pixel value.

The normalized image $F(u,v)_{norm}$ (Fig. 5, right) displays the density of spatial frequencies in the processed array.

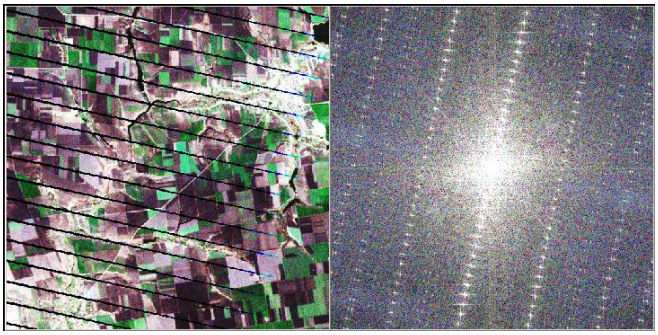

Fig. 5. A fragment of the Landsat-7 satellite image dated March 12, 2020

512x512 pixels (left) and its Fourier transform (right)

Filtration results when using various masks are shown in Fig. 6. As can be seen from the figure, during filtering by the Fourier transform, noise suppression is also associated with a decrease in spatial resolution and radiometric distortions but to a much lesser extent than by convolution filters. A better wedge-shaped mask provided the best interference filtering with minimal artifacts (Fig. 6 below).

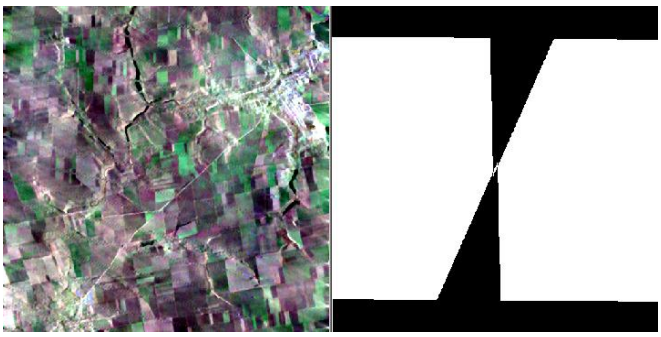

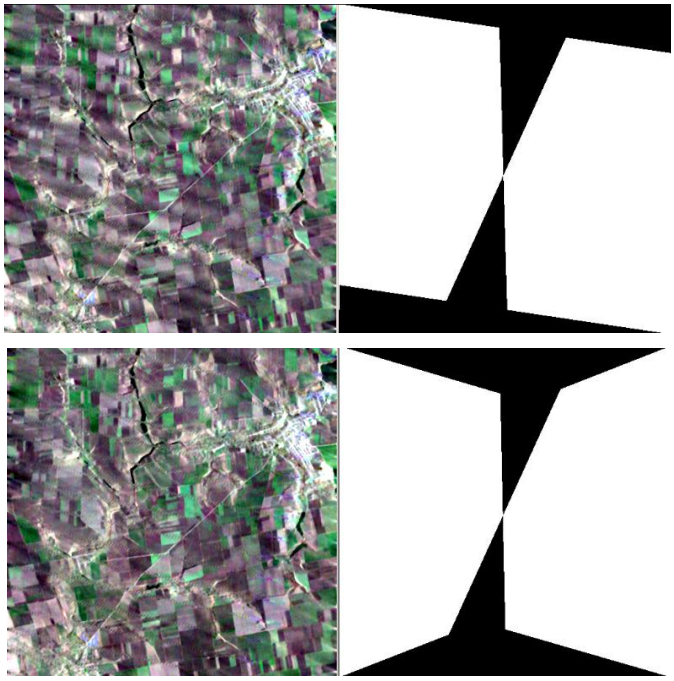

Fig. 6. Filtering results of the selected image fragment (left)

and masks used for filtration (right)

To correct radiometric distortions introduced directly by the Fourier transform, the histogram equalization operation is performed using the original image as a reference.

The results of processing Landsat-7 images for other territories and survey dates also confirmed the rather high efficiency of the proposed filtering method in comparison with the traditional one [20].

CONCLUSIONS

An alternative instrument distortions correction method for the ETM + scanner on Landsat-7 multispectral satellite images using fast Fourier transform is proposed. The visual analysis results of the processed images showed a high-quality suppression of instrument distortion of the ETM + scanner compared to other methods.

Experimental testing of the proposed method on many images confirmed the good repeatability and high stability of the algorithms used. The developed technology can also be successfully used for the correction of spatial periodic instrument distortions in archived satellite images obtained by using other optical and mechanical scanners.

REFERENCES

[1] (n.d.). Retrieved from https://blamannen.wordpress.com/2011/07/12/destripe-landsat-7-etm-some-thoughts/

[2] (n.d.). Retrieved from https://gis-lab.info/forum/viewtopic.php?t=4357

[3] (n.d.). Retrieved from https://yceo.yale.edu/how-fill-gaps-landsat-etm-images

[4] (n.d.). Retrieved from https://landsat.usgs.gov/sites/default/files/documents/SLC_Gap_Fill_Methodology.pdf

[5] (n.d.). Retrieved from http://landsat.usgs.gov/using_Landsat_7_data.php.

[6] D., M., R., T., O., A., & A., P. (2018). *Satellite monitoring of the drought consequences via medium and high resolution multispectral images* (Vol. 18). doi:10.5593/sgem2018/4.2/S19.075

[7] D.K., M., O.I., P., V.I., V., & Y.I., B. (2007). *Remote Sensing and GIS Application for Environmental Monitoring and Accidents Control in Ukraine.* doi:10.1007/978-1-4020-6438-8_16

[8] D.K., M., V.I., V., & E.I., B. (2004). *Filtration of Radiometric Interference with a Space-Periodic Structure.* doi:10.1615/JAutomatInfScien.v36.i6.20

[9] D.K., M., V.V., H., & V.V., V. (2018). *Automated recognition of vegetation and water bodies on the territory of megacities in satellite images of visible and IR bands.* doi:10.5194/isprs-annals

[10] Dolinets, J., & Mozgovoy, D. (2009). *Training of specialists in the field of Earth remote sensing.* doi:10.1016/j.actaastro

[11] *ERDAS Imagine Tour Guide.* (n.d.).

[12] *Filling the Gaps to use in Scientific Analysis.* (n.d.). Retrieved from http://landsat.usgs.gov/sci_an.php.

[13] *Gap Fill for Landsat 7 images.* (2012).

[14] O.L., M., D.K., M., & V.S., K. (2011). *Efficiency increasing methods for orbital satellite survey of randomly located areas.*

[15] *Removing stripes from Landsat-7.* (n.d.). Retrieved from imageshttps://community.esri.com/ thread/164902

[16] V., M. D. (2019). *Information Technology of Satellite Image Processing for Monitoring of Floods and Drought.* doi:https://doi.org/10.1007/978-3-030-33695-0_32.

[17] V.V., H., D.K., M., & V.V., V. (2017). *Satellite monitoring of deforestation as a result of mining.*

[18] V.V., H., D.K., M., V.V., S., & I.M., U. (2019). *All-weather monitoring of oil and gas production areas using satellite data.* doi:10.29202/nvngu/2019-6/20

[19] V.V., H., D.K., M., V.V., V., & O.O, K. (2017). *Satellite Monitoring of Consequences of Illegal Extraction of Amber in Ukraine.*

[20] V.V., H., Vik.V., H., D.K., M., & V.V., V. (2016). *Satellite technology of the forest fires effects monitoring.*